arXiv:2105.00943v2 [cond-mat.dis-nn] 23 Feb 2022

Geometry, Topology and Simplicial Synchronization

Ana Paula Millán, Juan G. Restrepo, Joaquín J. Torres and Ginestra Bianconi

Abstract Simplicial synchronization reveals the role that topology and geometry have in determining the dynamical properties of simplicial complexes. Simplicial network geometry and topology are naturally encoded in the spectral properties of the graph Laplacian and of the higher-order Laplacians of simplicial complexes. Here we show how the geometry of simplicial complexes induces spectral dimensions of the simplicial complex Laplacians that are responsible for changing the phase diagram of the Kuramoto model. In particular, simplicial complexes displaying a non-trivial simplicial network geometry cannot sustain a synchronized state in the infinite network limit if their spectral dimension is smaller or equal to four. This theoretical result is here verified on the Network Geometry with Flavor simplicial complex generative model displaying emergent hyperbolic geometry. On its turn simplicial topology is shown to determine the dynamical properties of the higher-order Kuramoto model. The higher-order Kuramoto model describes synchronization of topological signals, i.e., phases not only associated with the nodes of a simplicial complexes but associated also to higher-order simplices, including links, triangles and so on. This model displays discontinuous synchronization transitions when

Ana Paula Millán
Amsterdam UMC, Vrije Universiteit Amsterdam, Department of Clinical Neurophysiology and MEG Center, Amsterdam Neuroscience, De Boelelaan 1117, Amsterdam, The Netherlands. e-mail: a.p.millanvidal@amsterdamumc.nl

Juan G. Restrepo
Department of Applied Mathematics, University of Colorado at Boulder, Boulder, CO 80309, USAe-mail: juanga@colorado.edu

Joaquín J. Torres
Departamento de Electromagnetismo y Física de la Materia and Instituto Carlos I de Física Teórica y Computacional, Universidad de Granada, 18071, Granada, Spain e-mail: jtorres@onsager.ugr.es

Ginestra Bianconi
School of Mathematical Sciences, Queen Mary University of London
The Alan Turing Institute, The British Library, London, UK e-mail: ginestra.bianconi@gmail.com

topological signals of different dimension and/or their solenoidal and irrotational projections are coupled in an adaptive way.

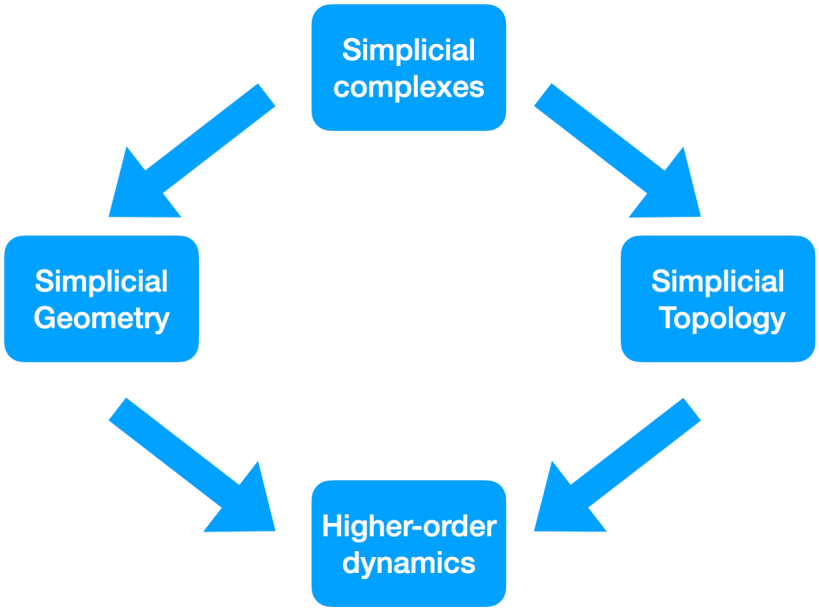


Fig. 1 Simplicial complexes encode the rich simplicial network topology and geometry of data and models, which strongly affects the higher-order dynamics. In this chapter we will see how this interplay between structure and dynamics can enrich our understanding of synchronization dynamics defined on simplicial complexes.

1 Introduction

The interplay between structure and dynamics of complex networks [1, 2, 3] has been at the forefront of network theory since the beginning of the field. In this context it has been found that the combinatorial and statistical properties of complex networks have unexpected effects on dynamics. For instance, a scale-free degree distribution changes the phase diagram of a wide range of dynamical processes including percolation, epidemic spreading, and the Ising model. The recent interest on higher-order networks [4, 5, 6, 7] provides an opportunity to bring a fresh perspective to this subject. Indeed, higher-order networks, and in particular simplicial complexes, constitute the ideal mathematical framework to capture the simplicial network topology and geometry of data. Here we reveal that the network topology and geometry of simplicial complexes can be crucial to define higher-order dynamics. The dynamical process considered in this chapter is synchronization [8, 9, 10], captured by

the Kuramoto model [11] and the recently introduced higher-order Kuramoto model [12]. The dynamical properties of these dynamical processes will be shown to be highly dependent on the spectral properties [13, 14] of the simplicial complexes [15, 16, 17, 18, 19] on which they are defined. The main message of this chapter is summarized in Figure 1, which highlights the role of network topology and network geometry in shaping higher-order network dynamics. In particular, in this chapter we will disclose how the spectral properties of simplicial complexes are foundational to reveal the relation between higher-order network geometry, topology and dynamics. Note that while our approach to simplicial synchronization is based on simplicial network geometry and topology, other approaches based on a combinatorial definition of higher-order interactions have been pursued in the literature [20, 21, 22], as covered by the Skardal and Arenas chapter of this book.

2 Simplicial complex models

Simplicial network models are ideal to test, in a well-controlled setting, the interplay between simplicial network geometry, topology and dynamics. Here we focus in particular on two large classes of simplicial complex models with very distinct structural properties: the Network Geometry with Flavor (NGF) [16, 17, 18, 19] and the configuration model of simplical complexes [15] (see schematic illustrations of the two models in Figure 2). These models are implemented in codes available at the repository [23].

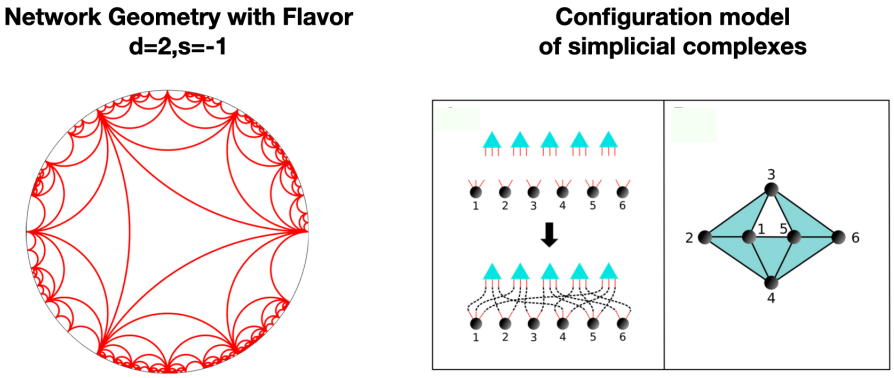


Fig. 2 Schematic representation of the two classes of simplicial complex models considered in this work. The Network Geometry with Flavor is a model of growing simplicial complexes describing emergent hyperbolic network geometries. The left panel shows a realization of the NGF simplicial complex of dimension $d = 2$ and flavor $s = -1$. The configuration model of simplicial complexes (right panel) is a maximum entropy model enforcing a given sequence of generalized degrees of the nodes. Right panel reprinted with permission from Ref. [15]. ©Copyright (2016) by the American Physical Society.

2.1 The Network Geometry with Flavor (NGF)

The Network Geometry with Flavor (NGF) [16, 17, 18, 19] is a general mathematical framework for growing simplicial complexes that displays emergent hyperbolic network geometry. In other words, the NGF model generates simplicial complexes with hyperbolic geometry that evolve following purely combinatorial and stochastic rules that do not make any use of the natural hyperbolic embedding of the simplicial complexes.

The NGFs are simplicial complexes characterized by two main parameters: the dimension of the simplicial complex d and the *flavor* s which is a parameter that takes values $s \in \{-1, 0, 1\}$. The NGFs are generated by a dynamical process which starting at time $t = 1$ from a single d-dimensional simplex proceeds at each time $t > 1$ by adding a new d-dimensional simplex to the simplicial complex. The new d-dimensional simplex includes one new node and is glued to a $(d-1)$-dimensional face α of the existing simplicial complex chosen according to the probability

$$\Pi_\alpha = \frac{1 - s + s k_{d,d-1}(\alpha)}{\sum_{\alpha'} 1 - s + s k_{d,d-1}(\alpha')}, \tag{1}$$

where $k_{d,d-1}(\alpha)$ indicates the generalized degree [15] of a $(d-1)$-dimensional face α, i.e., the number of d-dimensional simplices incident to the $(d-1)$-dimensional face α. This model generates emergent hyperbolic simplicial complexes which satisfy Gromov criteria [24] of hyperbolicity and are δ-hyperbolic with $\delta = 1$ for every value of the flavor s [25]. Moreover, for flavor $s = -1$ the generated simplicial complexes form d-dimensional hyperbolic manifolds [17]. The network skeleton of the NGFs are small world, display hierarchical community structure and are scale-free for $d \geq 2 - s$ [16, 17, 18]. Interestingly, in the case $d = 1$ and $s = 1$ the NGF reduces to the Barabási-Albert model, and for $d = 1$ and $s = -1$ the NGF reduces to random Apollonian networks.

This model can be generalized in different directions. Instead of considering simplicial complexes, one can use a similar model to generate cell complexes by gluing together convex regular polytopes [18]. Another possibility is to consider weighted simplicial complexes or to allow any new node to be incident to more than one d-dimensional simplex [19]. Finally, the faces can be assigned a fitness that can be used to modulate the attachment probability Π_α causing topological phase transitions for certain fitness distributions [16, 17].

2.2 Configuration model of simplicial complexes

The configuration model of simplicial complexes [15] is a maximum entropy model of pure d-dimensional simplicial complexes. A pure d-dimensional simplicial complex $\mathcal{K}$ can be fully encoded in a $(d+1)$-dimensional adjacency tensor indicating the presence of each d-dimensional facet of the simplicial complex. In particular

adjacency tensor **a** has elements $a_\alpha = 1$ if the d-dimensional simplex α is present in the simplicial complex, otherwise $a_\alpha = 0$.

The configuration model of simplicial complexes [15] is the least biased ensemble of simplicial complexes with a given generalized degree sequence of the nodes

$$\mathbf{k}_{d,0} = \{k_{d,0}(1), k_{d,0}(2), \dots k_{d,0}(N)\} \tag{2}$$

where $k_{d,0}(i)$ indicates the generalized degree of the node i, i.e., the number of d-dimensional complexes of the node $i \in \{1, 2, \dots, N\}$.

The configuration model of simplicial complexes is fully characterized by the probability $P(\mathcal{K})$ assigned to each pure d-dimensional simplicial complex $\mathcal{K}$ of N nodes. The probability $P(\mathcal{K})$ maximizes the entropy S of the simplicial complex ensemble

$$S = -\sum_{\mathcal{K}} P(\mathcal{K}) \ln P(\mathcal{K}), \tag{3}$$

given the constrain that each node i has generalized degree $k_{d,0}(i)$, i.e.,

$$\sum_{\alpha \in Q_d(N)|i\subset\alpha} a_\alpha = k_{d,0}(i), \tag{4}$$

where $Q_d(N)$ indicates the set of all possible d-dimensional simplices of a simplicial complex formed by N nodes. Therefore the configuration model of simplicial complexes is characterized by the uniform distribution

$$P(\mathcal{K}) = \frac{1}{\mathcal{N}} \prod_{i=1}^{N} \delta\left(\sum_{\alpha \in Q_d(N)|i\subset\alpha} a_\alpha, k_{d,0}(i) \right), \tag{5}$$

where here and in the following $\delta(a, b)$ indicates the Kronecker delta. In Ref. [15] the Authors proposed an algorithm for sampling simplicial complexes from this ensemble. This algorithm [23] uses the mapping of simplicial complexes to factor graphs. The configuration model of simplicial complexes is a very valuable null model of simplicial complexes, and provides an ideal benchmark to study dynamical processes on higher-order networks.

3 Laplacians

3.1 Graph Laplacian

The graph Laplacian describes linear diffusion on a network and it is an important operator that encodes the interplay between network structure and dynamics [3, 26]. The graph Laplacian can also capture the underlying network geometry of the

skeleton of a simplicial complex, i.e., of the network obtained from the simplicial complex by retaining only its nodes and links.

The graph Laplacian $\boldsymbol{L}_{[0]}$ is the discrete version of the Laplacian operator defined on continuous functions. The graph Laplacian of a network with $N_{[0]}$ nodes is a $N_{[0]} \times N_{[0]}$ matrix of elements

$$\left[L_{[0]}\right]_{ij} = k_i \delta(i,j) - a_{ij}, \tag{6}$$

where k_i is the degree of node i and a_{ij} are the elements of the adjacency matrix of the network. In some cases it is useful to consider a generalization of this operator called the normalized Laplacian $\hat{\boldsymbol{L}}_{[0]}$ that has elements

$$\left[\hat{L}_{[0]}\right]_{ij} = \delta(i,j) - \frac{a_{ij}}{k_i}. \tag{7}$$

For instance, the normalized Laplacian is commonly employed to describe random walk dynamics on a network.

Both the standard and the normalized Laplacians have real eigenvalues $0 = \lambda_1 \leq \lambda_2 \leq \ \ldots \ \leq \lambda_{N_{[0]}}$. The density of eigenvalues is described by the spectral density,

$$\rho(\lambda) = \frac{1}{N_{[0]}} \sum_{i=1}^{N_{[0]}} \tilde{\delta}(\lambda - \lambda_i), \tag{8}$$

where $\tilde{\delta}\,(x)$ indicates the delta function. The eigenvectors of the normalized Laplacian also encode relevant properties of the underlying network.

3.2 Spectral dimension

For many complex networks, the smallest non-zero eigenvalue (also called Fiedler eigenvalue) λ_2 remains finite as the network size increases. In this case, the network is said to have a *spectral gap*. On the contrary, if $\lambda_2 \to 0$ as $N \to \infty$, and the density of eigenvalues $\rho(\lambda)$ scales as

$$\rho(\lambda) \propto \lambda^{d_S^{[0]}/2-1}, \tag{9}$$

for $\lambda \ll 1$, the network is said to present a *spectral dimension* $d_S^{[0]}$ [27, 26, 28]. The spectral dimension can be interpreted as the perceived dimension of the network by diffusion processes, and it is a notable feature of networks with an underlying geometrical nature. This is a definition of dimension that is alternative to the Hausdorff dimension d_H characterizing the scaling of the diameter D of a network with the network size N, i.e., $D \propto N^{1/d_H}$.

For Euclidean lattices of dimension d, the spectral dimension coincides with the Hausdorff dimension and we have $d_S^{[0]} = d_H = d$. However, in general the spectral

dimension of a network skeleton of a simplicial complex does not have to coincide with the topological dimension of the simplicial complex, nor with its Hausdorff dimension [29, 27, 30, 25].

While Euclidean lattices display a finite spectral dimension, random graphs and the configuration model of networks are instead characterized by a finite spectral gap. The presence of a finite spectral gap indicates the mean-field nature of the network interactions, and the absence of a clear notion of locality for these networks. Interestingly, also the configuration model of simplicial complexes displays a finite spectral gap.

Remarkably, the emergent network geometry of NGF reveals itself on their significant spectral properties. Indeed the NGF network skeletons, together with other small-world of simplicial complexes [31], have a finite spectral dimension whose value can be tuned according to the different control parameters [18] although the NGFs are small world, i.e., they have an infinite Hausdorff dimension $d_H = \infty$. For

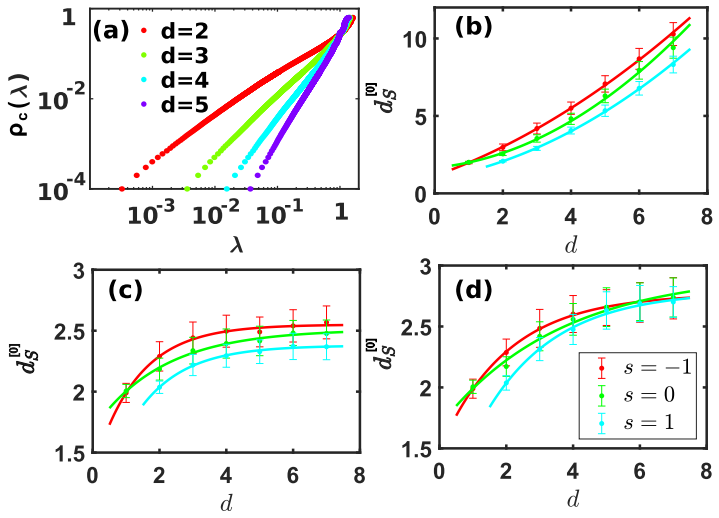


Fig. 3 Spectral dimension of NGF networks. Panel (a) The cumulative distribution $\rho_c(\lambda)$ of eigenvalues of the NGF with flavor $s = -1$ is shown for dimension $d = 2, 3, 4, 5$. The power-law scaling of $\rho_c(\lambda)$ observed for small values of λ indicates that the skeleton of NGF has a finite spectral dimension. **Panels (b-d)** The fitted spectral dimension $d_S^{[0]}$ of the skeleton of NGF simplicial and cell complexes being formed by simplices (panel (**b**)), hypercubes (panel (**c**)) and orthoplexes (panel (**c**)), is shown for values of the flavor $s \in \{-1, 0, 1\}$ as indicated in the legend of panel (**d**). Lines indicate best fit of the $d_S^{[0]}$ versus d dependence using parabolic (panel (**b**)) and exponential (panels (**c**), (**d**)) functional forms. Data from Ref. [32] and Ref. [18]. Details of the fits are described in Ref. [18].

.

$s = -1$, NGF networks formed purely by d-dimensional simplices have $d_S^{[0]} \sim d$ for $d \in \{2, 3, 4\}$ as shown in Figure 3 [33]. More generally, for NGFs formed by regular polytopes, $d_S^{[0]}$ increases with the dimension d of the polytopes, and it saturates for

hypercubes and orthoplexes ($d_S^{[0]} \leq 3$) [32]. It was shown in Ref. [18] that a similar trend is observed for different flavours of the NGF networks: $d_S^{[0]}$ grows proportional to d^2 for simplicial NGF networks, whereas it saturates at a value $d_S^{[0]} = \bar{d}_S$ with $2 \leq \bar{d}_S \leq 3$ for hypercube and orthoplex NGF networks. Moreover, it was shown recently in Ref. [25] that, in a generalization of the NGF model in which different polytopes are glued together in the same higher-order network, the spectral dimension of the network skeleton can be continuously tuned as a function of the fraction of simplexes in the cell complex.

Thus, not only the dimension of the building blocks shapes the spectral dimension of the networks, but the specific nature and symmetry of these building blocks also play a role in the emerging spectral dimension of the network skeleton (see Figure 3).

3.3 Higher-order Laplacians

Important topological aspects of simplicial complexes are reflected in the spectral properties of the higher-order Laplacians that generalize the graph Laplacian to describe diffusion that occurs among higher-order simplices. The graph Laplacian describes diffusion occurring among nodes connected by links. Similarly the n-th order up-Laplacian describes the diffusion occurring among n-dimensional simplices connected by $(n+1)$-dimensional simplices and the n-th order down-Laplacian describes the diffusion occurring among n-dimensional simplices connected by $(n-1)$-dimensional simplices. The higher-order Laplacians capture the topology of simplicial complexes. For instance their spectrum encodes the Betti numbers, i.e., the number of n-dimensional cavities of the simplicial complex.

The higher-order Laplacians are defined in terms of the incidence matrices of the simplicial complex which represent the boundary operators playing a fundamental role in algebraic topology.

Here we provide a brief introduction to the necessary elements of algebraic topology needed to define higher-order Laplacians.

We consider a d-dimensional simplicial complex formed by $N_{[n]}$ simplices of dimension n. The simplices of the simplicial complexes are associated with an orientation induced by the labelling of the nodes so that the link $[i, j]$ has a positive orientation if $j > i$ and so on (see Figure 4).

We consider algebraic entities called n-chains that are linear combinations of n-dimensional simplices with coefficients in $\mathbb{Z}$. In a less informal definition n-chains are the elements of a free abelian group C_n with basis on the n-simplices of the simplicial complex. The boundary map is a linear map $\partial_n : C_n \to C_{n-1}$ defined by its action on each simplex $\alpha = [i_0, i_1, i_2 \ldots, i_n]$. In particular the boundary map associates to every n-dimensional simplex $\alpha = [i_0, i_1, i_2 \ldots, i_n]$ a linear combination of the $(n-1)$-dimensional oriented faces at its boundary, given by

$$\partial_n[i_0, i_1 \ldots, i_n] = \sum_{p=0}^{n} (-1)^p [i_0, i_1, \ldots, i_{p-1}, i_{p+1}, \ldots, i_n]. \tag{10}$$

It follows that the image of the boundary operator ∂_n are the $(n-1)$-chains that are at the boundary of n-chains. For instance we have

$$\partial_2([1,2,3]) = [1,2] + [2,3] - [1,3], \tag{11}$$

i.e., the image of a triangle is the linear combination of the links at its boundary with the correct orientation. Additionally, from this definition it is also easy to see that a cyclic n-chain is in the kernel of the boundary map ∂_n independently of whether the cyclic n-chain is the boundary of a $(n+1)$-chain. For instance we have

$$\partial_1([1,2] + [2,3] - [1,3]) = [2] - [1] + [3] - [2] - [3] + [1] = 0, \tag{12}$$

whether the simplex $[123]$ belongs to the simplicial complex or not. One important topological property of the boundary operator is that the "boundary of a boundary is null" which implies

$$\text{im } \partial_{n+1} \subseteq \ker \partial_n \tag{13}$$

or equivalently

$$\partial_n \partial_{n+1} = 0. \tag{14}$$

For instance we have

$$\partial_1 \partial_2 [1,2,3] = \partial_1([1,2] + [2,3] - [1,3]) = 0. \tag{15}$$

The boundary map ∂_n can be represented by a $N_{[n-1]} \times N_{[n]}$ incidence matrix $\mathbf{B}_{[n]}$ if we adopt as a basis of the space C_n an ordered set of the n-dimensional simplices α, and as a basis of the space C_{n-1} an ordered set of the $(n-1)$-dimensional simplices $\hat{\alpha}$.

If the basis of n-chains C_n is given by the n-simplices $\{\alpha_1, \alpha_2, \ldots \alpha_s \ldots\}$ and the basis of $(n-1)$-chains C_{n-1} is given by the $(n-1)$-simplices $\{\hat{\alpha}_1, \hat{\alpha}_2, \ldots \hat{\alpha}_r \ldots\}$ the action of the boundary map over any arbitrary n-dimensional simplex $\alpha_s = [i_0, i_1 \ldots, i_n]$ given by Eq. (10) can be expressed as

$$\partial_n \alpha_s = \sum_{r=1}^{N_{n-1}} [B_{[n]}]_{rs} \hat{\alpha}_r. \tag{16}$$

This equation fully determines the incidence matrices $\mathbf{B}_{[n]}$. Since we have seen that the "boundary of a boundary is null" then the incidence matrices follow $\mathbf{B}_{[n]}\mathbf{B}_{[n+1]} = \mathbf{0}$ and also $\mathbf{B}^{\top}_{[n+1]}\mathbf{B}^{\top}_{[n]} = \mathbf{0}$. As an example we can consider the simplicial complex shown in Figure 4 whose incidence matrices are given by

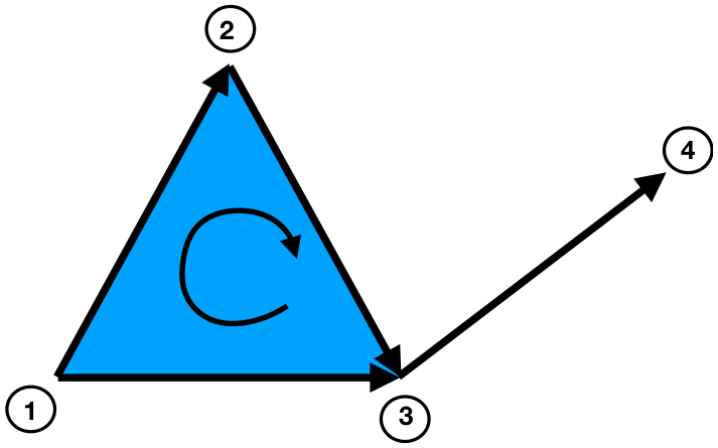


Fig. 4 Example of oriented simplicial complex. This illustrates an example of a 2-dimensional oriented simplicial complex having associated incidence matrices given by Eqs. (17). Reprinted figure with permission from Ref. [12]. ©Copyright (2020) by the American Physical Society.

.

$$\mathbf{B}_{[1]} = \begin{array}{c|cccc} & [1,2] & [1,3] & [2,3] & [3,4] \\ \hline [1] & -1 & -1 & 0 & 0 \\ [2] & 1 & 0 & -1 & 0 \\ [3] & 0 & 1 & 1 & -1 \\ [4] & 0 & 0 & 0 & 1 \end{array}, \quad \mathbf{B}_{[2]} = \begin{array}{c|c} & [1,2,3] \\ \hline [1,2] & 1 \\ [1,3] & -1 \\ [2,3] & 1 \\ [3,4] & 0 \end{array}. \tag{17}$$

The graph Laplacian can be expressed in terms of the incidence matrix $\mathbf{B}_{[1]}$ of the graph as

$$\mathbf{L}_{[0]} = \mathbf{B}_{[1]}\mathbf{B}_{[1]}^{\top}. \tag{18}$$

Similarly, in a simplicial complex the higher-order Laplacian $\mathbf{L}_{[n]}$ (with $n > 0$) [34, 35, 14] is the $N_{[n]} \times N_{[n]}$ matrix defined as

$$\mathbf{L}_{[n]} = \mathbf{L}_{[n]}^{[\text{down}]} + \mathbf{L}_{[n]}^{[\text{up}]}, \tag{19}$$

where

$$\mathbf{L}_{[n]}^{[\text{down}]} = \mathbf{B}_{[n]}^{\top}\mathbf{B}_{[n]}, \quad \mathbf{L}_{[n]}^{[\text{up}]} = \mathbf{B}_{[n+1]}\mathbf{B}_{[n+1]}^{\top}. \tag{20}$$

The n-Laplacian is positive semi-definite and, therefore, it has $N_{[n]}$ non negative eigenvalues $0 \leq \lambda_1 \leq \lambda_2 \leq \ldots \lambda_r \leq \ldots \leq \lambda_{N_{[n]}}$. A notable property of the spectrum of the n-th order Laplacian is that the degeneracy of zero eigenvalues is given by the n-th Betti number. Despite the fact that the construction of the higher-order Laplacians described above seems to rely on the choice of the orientations adopted for the simplices of the simplicial complex, it is possible to show that the higher-

order Laplacians are independent on the orientation of the simplices as long as such orientation is induced by the labeling of the nodes.

We note that also the up and the down Laplacians are positive semi-definite and that from the definition of these matrices it follows immediately than the non-zero eigenvalues in the spectrum of $\mathbf{L}_{[n]}^{[\mathrm{up}]}$ are the same as the non-zero eigenvalues in the spectrum of $\mathbf{L}_{[n]}^{[\mathrm{down}]}$.

By considering the property of the incidence matrices such that $\mathbf{B}_{[n]}\mathbf{B}_{[n+1]} = 0$, it is possible to derive the Hodge decomposition of the space of n-chains, which reads

$$\mathbb{R}^{D_n} = \mathrm{img}(\mathbf{B}_{[n]}^{\top}) \oplus \ker(\mathbf{L}_{[n]}) \oplus \mathrm{img}(\mathbf{B}_{[n+1]}). \tag{21}$$

This implies that the higher-order Laplacian $\mathbf{L}_{[n]}$ can be simultaneously diagonalized with the n-th order up and n-th order down Laplacian and that the non-zero eigenvectors of $\mathbf{L}_{[n]}$ are either non-zero eigenvector of $\mathbf{L}_{[n]}^{[\mathrm{down}]}$ or non-zero eigenvectors of $\mathbf{L}_{[n]}^{[\mathrm{up}]}$. Therefore there is a basis in which $\mathbf{L}_{[n]}$, $\mathbf{L}_{[n]}^{[\mathrm{down}]}$ and $\mathbf{L}_{[n]}^{[\mathrm{up}]}$ have diagonal form given by

$$\mathbf{U}^{-1}\mathbf{L}_{[n]}\mathbf{U} = \begin{pmatrix} \mathbf{D}_{[n]}^{[\mathrm{down}]} & \mathbf{0} & \mathbf{0} \\ \mathbf{0} & \mathbf{0} & \mathbf{0} \\ \mathbf{0} & \mathbf{0} & \mathbf{D}_{[n]}^{[\mathrm{up}]} \end{pmatrix}, \ \mathbf{U}^{-1}\mathbf{L}_{[n]}^{[\mathrm{down}]}\mathbf{U} = \begin{pmatrix} \mathbf{D}_{[n]}^{[\mathrm{down}]} & \mathbf{0}\,\mathbf{0} \\ \mathbf{0} & \mathbf{0}\,\mathbf{0} \\ \mathbf{0} & \mathbf{0}\,\mathbf{0} \end{pmatrix}, \ \mathbf{U}^{-1}\mathbf{L}_{[n]}^{[\mathrm{up}]}\mathbf{U} = \begin{pmatrix} \mathbf{0}\,\mathbf{0} & \mathbf{0} \\ \mathbf{0}\,\mathbf{0} & \mathbf{0} \\ \mathbf{0}\,\mathbf{0} & \mathbf{D}_{[n]}^{[\mathrm{up}]} \end{pmatrix},$$

where $\mathbf{D}_{[n]}^{[\mathrm{up}]}$ and $\mathbf{D}_{[n]}^{[\mathrm{down}]}$ are diagonal matrices having positive diagonal elements.

3.4 Higher order spectral dimension

The notion of spectral dimension (see section 3.2) can be generalized to n-order up-Laplacians with important consequences for higher-order simplicial complex dynamics. Here, we will focus on the model of NGF simplicial complexes introduced in section 2.1. In section 3.2, we have shown that the graph Laplacian of NGFs displays a finite spectral dimension $d_S^{[0]}$ [18, 33, 32]. Interestingly, higher-order up-Laplacians $\mathbf{L}_{[n]}^{[\mathrm{up}]}$ and the higher-order down-Laplacians $\mathbf{L}_{[n]}^{[\mathrm{down}]}$ of NGFs also display a finite spectral dimension.

In particular, the higher-order up-Laplacians of NGFs display a finite spectral dimension $d_S^{[n]}$ depending on the order n, the dimension of the simplicial complex d and the flavor parameter s [13]. Therefore, we can define different spectral dimensions for $0 < n < d - 1$. In order to show this remarkable geometrical property of NGFs in Figure 5 we provide numerical evidence of the scaling of the cumulative density of non-zero eigenvalues $\rho_c^{\mathrm{up}}(\lambda)$ of the $\mathbf{L}_{[n]}^{[\mathrm{up}]}$ with λ for $\lambda \ll 1$, given by

$$\rho_c^{[\mathrm{up}]}(\lambda) \propto \lambda^{d_S^{[n]}/2}, \tag{22}$$

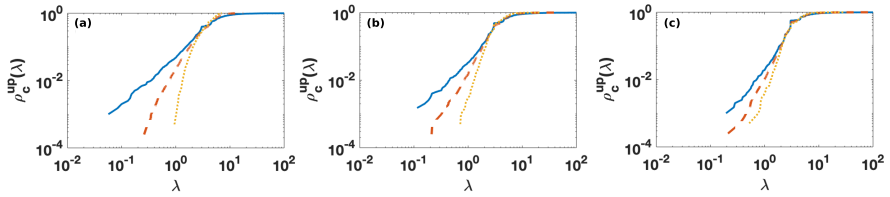


Fig. 5 The cumulative density of non-zero eigenvalues $\rho_c^{up}(\lambda)$ of the $\mathbf{L}_{[n]}^{[\mathrm{up}]}$ for NGF of dimension $d = 3$ and flavor $s = -1$ (panel (**a**)), $s = 0$ (panel (**b**)), and $s = 1$ (panel (**c**)) for $n = 0$ (blue solid lines), $n = 1$ (red dashed lines), $n = 2$ (yellow dotted lines) and $n = 3$ (purple dot-dashed lines). Considered NGFs sizes are $N_{[0]} = 2000$ nodes, $N_{[1]} = 5994$ links, $N_{[2]} = 5992$ triangles, and $N_{[3]} = 1997$ tetrahedra. Adapted figure from [13].

for different value of the order n of the up-Laplacian, and the flavor s of the NGF. It follows that an NGF model is not characterized by a single spectral dimension, i.e., the spectral dimension $d_S^{[0]}$ of the graph Laplacian, rather the NGF simplicial complexes have a higher-order network geometry encoded in a vector of spectral dimensions

$$\mathbf{d}_S = \left(d_S^{[0]}, d_S^{[1]}, d_S^{[2]} \ldots, d_S^{[d-1]}\right). \tag{23}$$

Consequently, the diffusion dynamics defined on simplices of different order n of the same NGF simplicial complex can be significantly different [36]. We finally note that for deterministic Apollonian and pseudo-fractal simplicial complexes that constitute the deterministic counterpart of NGF simplicial complexes, the higher-order spectral dimension can be predicted analytically by the real-space renormalization group [37] showing that the higher-order spectral dimension of these structures depends on the order n and remains finite as long as $0 \leq n < d - 1$.

4 Simplicial synchronization

Synchronization is a fundamental dynamical state observed in a wide variety of complex systems and capturing among other phenomena important aspects of brain dynamics and circadian rhythms. The Kuramoto model [11, 8, 38, 9, 10] is a stylized model that explains how coupled oscillators, that in absence of interactions would have different intrinsic frequencies, can start to follow a collective coherent motion when their coupling constant σ, measuring the strength of their interaction, is larger than a critical value σ_c also called *synchronization threshold*.

In order to model the coupling between the oscillators the Kuramoto model considers a network of $N_{[0]}$ nodes and associates a phase θ_i to each node $i \in \{1, 2, \ldots, N_{[0]}\}$ of the network. Therefore in the Kuramoto model, the dynamical state of the network is determined by the vector $\boldsymbol{\theta}$ of phases associated with its nodes

given by

$$\boldsymbol{\theta} = (\theta_1, \theta_2, \ldots, \theta_{N_{[0]}})^\top. \tag{24}$$

Each phase θ_i describes the dynamical state of an oscillator that in absence of interactions oscillates at an intrinsic frequency ω_i drawn independently from a distribution $g(\omega)$. Common choices for $g(\omega)$ are the unimodal Gaussian or Lorentzian distributions.

The equations determining the dynamics of the phases associated with the nodes include an important contribution indicating the coupling among the phases of neighbour nodes. This coupling term has a strength modulated by the coupling constant σ. In , it is assumed that this contribution expresses the tendency of the phase of any given node to oscillate together with the phases of its neighbour nodes. The resulting standard Kuramoto dynamics is captured by the differential equations

$$\dot{\theta}_i = \omega_i + \sigma \sum_{j=1}^{N_{[0]}} a_{ij} \sin\left(\theta_j - \theta_i\right), \tag{25}$$

valid for every node i of the network, where a_{ij} is the generic element of the adjacency matrix of the network. The level of synchronization in the system is measured by the Kuramoto order parameter,

$$Z_0 = R_0 \mathrm{e}^{\mathrm{i}\Theta} = \frac{1}{N} \sum_{j=1}^{N_{[0]}} \mathrm{e}^{\mathrm{i}\theta_j}, \tag{26}$$

where R_0 and Θ are both real and where $0 \leq R_0 \leq 1$ measures the overall coherence and $\Theta = \Theta(t)$ is the phase of global oscillations.

The relation between the Kuramoto model and the graph Laplacian of the underlying network is revealed when the Kuramoto model is linearized for $|\theta_i - \theta_j| \ll 1$ for every pair of neighbour nodes (i, j). In this limit the Kuramoto model can be shown to be described by the system of equations

$$\dot{\boldsymbol{\theta}} = \boldsymbol{\omega} - \sigma \mathbf{L}_{[0]} \boldsymbol{\theta}, \tag{27}$$

where $\boldsymbol{\omega}$ indicates the vector of elements ω_i with $i \in \{1, 2, \ldots, N_{[0]}\}$.

The Kuramoto model has been analytically solved only on a fully connected network, although important progress has been made in understanding the Kuramoto model in random complex networks [9, 39, 40],

In the fully connected network and in random networks the Kuramoto model displays a second order phase transition at the synchronization threshold $\sigma = \sigma_c$ when the number of nodes goes to infinity, i.e., $N_{[0]} \to \infty$. For $\sigma < \sigma_c$ the Kuramoto model is in an incoherent state characterized by having a zero order parameter $R_0 = 0$. For $\sigma > \sigma_c$ the Kuramoto model is in a coherent state characterized by a non-zero order parameter $R_0 > 0$ [38, 8, 9, 10].

In this chapter we show how the network geometry and topology of simplicial complexes, directly acting on the spectral properties of the graph Laplacian and the higher-order Laplacians, can dramatically change the dynamical properties of the synchronization process on higher-order networks.

- **Simplicial network geometry and the Kuramoto model.** First we will illustrate how the phase diagram of the Kuramoto model changes when the model is defined on the skeleton of simplicial complexes with distinct higher-order network geometry. We have previously introduced the finite spectral dimension $d_S^{[0]}$ of the graph Laplacian as a fundamental observable of the higher-order network geometry of networks and simplicial complexes. In the following we will discuss how the dynamics of the Kuramoto model depends on $d_S^{[0]}$ revealing that network geometries have a more rich dynamics than random networks.
- **Simplicial network topology and the higher-order Kuramoto model.** Secondly we will reveal how the Kuramoto model can be considered as a limiting case of a much wider class of higher-order Kuramoto models describing coupling of topological signals. Topological signals are phases of oscillators associated not only to the nodes but also to higher-order simplices of a simplicial complex. For instance topological signals can be associated with both nodes and links of a simplicial complex as schematically described by Figure 4. In this case the dynamical state of a simplicial complex is captured by the vector $\boldsymbol{\theta}$ of the phases associated with the nodes (defined in Eq. (24)) and by the vector $\boldsymbol{\phi}$ of the phases

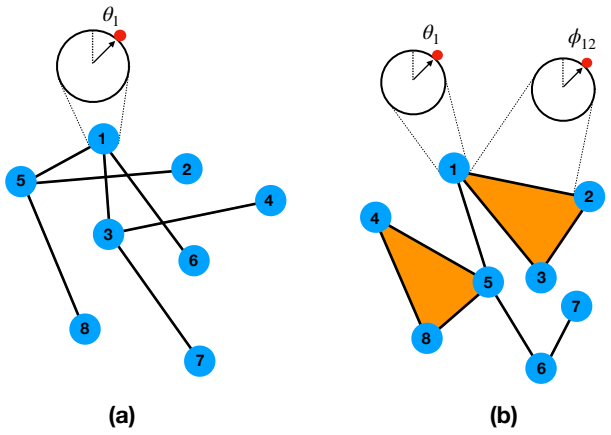


Fig. 6 Schematic representation of the Kuramoto model and the higher-order Kuramoto model capturing dynamics of topological signals. The Kuramoto model (panel (**a**)) captures the emergence of a synchronized state among coupled oscillators described by phases associated with the nodes of a network. The higher-order Kuramoto model (panel (**b**)) reveals the synchronization of topological signals on simplicial complexes, i.e., oscillators associated not only to the nodes of a simplicial complex, but also to higher-dimensional simplices such as links or triangles. Interestingly, topological signals of different dimension can co-exist and co-evolve and can be non-trivially coupled leading to simultaneous explosive transitions.

associated with the links of the simplicial complex given by

$$\boldsymbol{\phi} = \left(\phi_{\ell_1}, \phi_{\ell_2}, \ldots, \phi_{\ell_{N_{[1]}}}\right)^{\top}. \tag{28}$$

The phases associated with the links of the simplicial complexes are topological signals that have the potential to capture the dynamics of fluxes in brain networks [41] and biological transportation networks [42]. The newly formulated higher-order Kuramoto model opens new scenarios for characterizing how topology affects dynamics on higher-order networks and simplicial complexes. As we will discuss in Sec. V the higher-order Kuramoto model has a linearized dynamics described by the higher-order Laplacians of the simplicial complex, and can display the simultaneous explosive synchronization transition of the soleinodal and the irrotational component of topological signals and even the simultaneous explosive synchronization transition of topological signals of different dimensions.

5 Kuramoto model on simplicial network geometry

5.1 Synchronization on simplicial network skeletons with finite spectral dimension

In order to investigate the role that simplicial network geometry has on the Kuramoto model we explore the phase diagram of the normalized Kuramoto model on networks with finite spectral dimension [32]. Our theoretical results are then validated by simulations performed over the skeleton of the NGF with flavor $s = -1$. Indeed NGF with flavor $s = -1$ provide a very suitable benchmark to test our theoretical results as they display a spectral dimension $d_S^{[0]}$ that can be changed by tuning the dimension d of the simplicial complex [33].

The normalized Kuramoto model determines the dynamics of the phases $\boldsymbol{\theta}$ associated with the nodes of a network. The only difference with the standard Kuramoto model is that the coupling between the phase of a given node i and the phases of its neighbour nodes is normalized with the node degree k_i. Therefore, the normalized Kuramoto model is dictated by the differential equations

$$\dot{\theta}_i = \omega_i + \sigma \sum_{j=1}^{N_{[0]}} \frac{a_{ij}}{k_i} \sin\left(\theta_j - \theta_i\right), \tag{29}$$

where here and in the following we consider internal frequencies ω_i drawn independently from a normal distribution, i.e., $\omega_i \sim \mathcal{N}(0, 1)$. The normalization of the coupling term by the degree of the node i is a very efficient way to screen out the effects of the heterogeneity of the degrees of the nodes and single out only the effects due to the geometrical nature of the network of their interactions.

The linearized equation of the normalized Kuramoto model is therefore determined by the normalized Laplacian $\hat{\mathbf{L}}_{[0]}$ instead of the graph Laplacian $\mathbf{L}_{[0]}$, i.e.,

$$\dot{\boldsymbol{\theta}} = \boldsymbol{\omega} - \sigma \hat{\mathbf{L}}_{[0]} \boldsymbol{\theta}. \tag{30}$$

The analytical investigation of the stability of the synchronized phase indicates that the spectral dimension $d_S^{[0]}$ of the (normalized) graph Laplacian of the network plays a fundamental role for determining the phase diagram of the normalized Kuramoto model in the limit of infinite network size $N_{[0]} \to \infty$ [32]. Interestingly, we note that the spectral dimension of the graph Laplacian and the normalized graph Laplacian take the same value under very general regularity conditions of the network [28]. For the very heterogeneous NGF, numerical results show that the two spectral dimensions differ by a small amount as long as the topological dimension d is small. Depending on the value of the spectral dimension the phase diagram of the normalized Kuramoto model defined in the infinite network limit changes drastically [32]:

(1) For networks with finite spectral dimension $d_S^{[0]} \leq 2$, the Kuramoto model cannot synchronize and is found in the incoherent state for every value of the coupling constant σ.
(2) For networks with spectral dimension $2 < d_S^{[0]} \leq 4$, global synchronization is not achievable in the infinite network limit but an entrained state can be observed. Therefore it is possible the Kuramoto model can have a transition between an incoherent state and an entrained phase.
(3) Only for networks with spectral dimension $d_S^{[0]} > 4$ it is possible to see a synchronized phase.

These results reveal how the dynamics of the Kuramoto model depends on the simplicial network geometry on which is defined, and extend previous results valid on regular lattices of dimension d [43, 44].

5.2 Frustrated synchronization on Network Geometry with Flavor

The NGF constitutes a perfect model to investigate numerically the role that simplicial network geometry has on the dynamics of the Kuramoto model [33, 32]. Indeed, as we discussed previously, the NGF displays an emergent hyperbolic network geometry and for flavor $s = -1$ generates random hyperbolic manifolds. The simplicial network geometry of NGF is also reflected on their spectral properties. Specifically, NGFs have a finite spectral dimension $d_S^{[0]}$ which for flavor $s = -1$ and $d \in \{2, 3, 4\}$ can be approximated by $d_S^{[0]} \simeq d$. It follows that by changing the dimension d of the NGF with flavor $s = -1$ we can explore the dynamics of the Kuramoto model when the global synchronization state is not stable in the infinite network limit.

A computational finite size analysis of the Kuramoto model [33, 32] reveals, in agreement with the theoretical expectations, that for $d = 2$ and $d_S^{[0]} \simeq 2$, global

synchronization is never achieved for large network sizes. On the other hand, synchronization in NGFs with $d = 3$ and $d = 4$ and $d_S^{[0]} \simeq d$ is only possible for finite networks. In fact its onset occurs for higher couplings when the system size increases, revealing, in agreement with the theoretical expectation, that in the limit $N_{[0]} \to \infty$ this state is never achieved.

Interestingly, we observe that for NGF with $d = 3$ and $d = 4$ and $d_S^{[0]} \simeq d$ the Kuramoto model exhibits a phase with entrained synchronization that we call a phase of *frustrated synchronization* for a wide range of coupling values. In the *frustrated synchronization regime* the order parameter R_0 displays strong temporal fluctuations. This phase is observed on finite NGF between the incoherent state and the globally synchronized state, and for $d = 3$ a much broader regime of large fluctuations is observed than for the $d = 4$ case.

Interestingly, the frustrated synchronization phase of NGFs is not only characterized by strong temporal fluctuations of the global order parameter but displays also strong spatial fluctuations induced by the non-trivial hyperbolic network geometry of the NGF. As such, the frustrated synchronization phase can capture an important mechanism for inducing spatio-temporal fluctuations in brain dynamics.

The hyperbolic network geometry of NGF has a strong hierarchical nature that is responsible for the emergence of a relevant community structure. In order to study how the dynamics of the Kuramoto model is affected by the community structure of the NGFs, we define mesoscopic synchronization order parameters Z_{mod} that characterize the dynamical state of each community:

$$Z_{\text{mod}} = R_{\text{mod}} e^{i\Theta_{\text{mod}}} = \frac{1}{|C|} \sum_{j \in C} e^{i\theta_j}, \tag{31}$$

where C is the set of nodes in the community and $|C|$ the total number of nodes in said community. Figure 7b displays the trajectory of $Z_{\text{mod}} = Z_{\text{mod}}(t)$ in the complex plane for some exemplary modules of an NGF with flavour $s = -1$ in $d = 3$, for the coupling that leads to the largest fluctuations of R_0 as a function of time. As shown in the figure, different modules display different synchronization regimes and may oscillate at different frequencies. Due to the underlying geometrical structure of NGFs, these modules correspond to spatially localized regions.

We note here that the frustrated synchronization observed in NGF can be related with analogous phases observed in other hierarchical models [45, 46] where temporal fluctuations of the synchronization order parameter are observed. However, the combination of both temporal and spatial fluctuations is a specific property of the frustrated synchronization in NGF due to their rich simplicial network geometry.

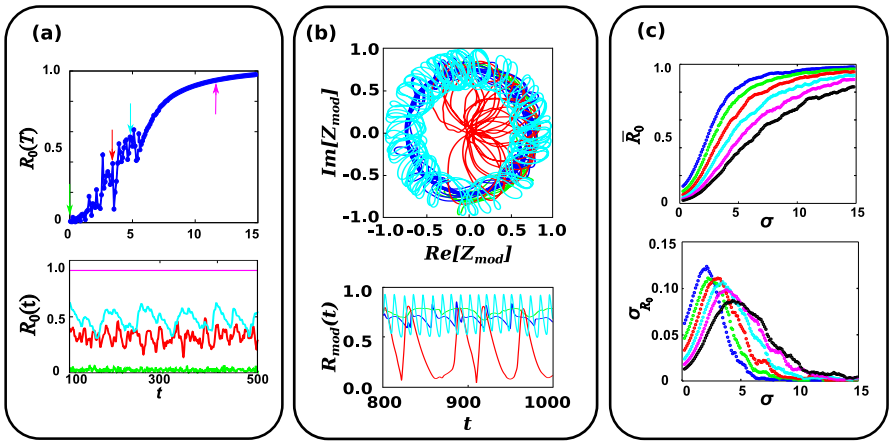


Fig. 7 Frustrated synchronization on NGF characterized by spatio-temporal fluctuations of the order parameter. Panel (a) The synchronization order parameter $R_0(T)$ calculated at time T is plotted versus the coupling constant σ revealing the regime of frustrated synchronization (top panel). The time series $R_0(t)$ are shown (bottom panel) for the values of the coupling constant σ indicated by arrows in the top panel. These time series reveal the temporal fluctuations of the order parameter in the frustrated synchronization regime. **Panel (b)** The spatial fluctuations of the order parameter in the frustrated synchronization regime are revealed by the local order parameter $Z_{\rm mod}$ of four different communities of the NGF calculated for $\sigma = 5$ (top panel). In this representation, a circular trajectory describes a situation of global oscillations of the nodes in the community, with constant $R_{\rm mod}(t)$. Random trajectories around the origin describe unsynchronized communities. Partially synchronized communities, on the other hand, may describe more complex trajectories. The bottom panel shows the corresponding time series of $R_{\rm mod}(t)$. **Panel (c)** Synchronization transition as given by the mean order parameter $\bar{R}_0$ averaged over time and its variance σ_{R_0}, as functions of σ, for different network sizes $N = 100$ (blue), 200, 400, ..., 3200 (black). The apparent onset of the synchronized regime is retarded to large values of the coupling constant σ for large network sizes, revealing that the NGF of dimension $d = 3$ cannot sustain a synchronized phase in the limit of infinite network sizes. All simulations reported in the figures are obtained for NGF of flavor $s = -1$, dimension $d = 3$ and number of nodes $N_{[0]} = 1600$. In panel (**a**) $T = 500$. Figure adapted from [33].

6 Higher-order Kuramoto model: a topological approach to synchronization

6.1 Synchronization of topological signals

Simplicial complexes are formed by nodes and higher-order simplices including links, triangles, tetrahedra, and so on. As such, simplicial complexes have the ability to sustain topological signals, i.e., dynamic variables not only associated with the nodes of their network skeleton but also associated with links, triangles, and so on [12, 47, 14]. Topological signals have the ability to capture dynamics associated with links, such as fluxes in brain networks [41] and biological transportation networks [42, 48].

Here we will present the higher-order Kuramoto model [12] that reveals how topological signals can undergo continuous and discontinuous synchronization transitions. Interestingly, we will observe that this synchronization transition can be detected only if the signals are filtered with the appropriate topological operators. Therefore, the model not only captures a new topological critical phenomenon but also prescribes a way to process real data in order to investigate whether this topological synchronization phenomenon can be observed in real systems such as the brain or biological transportation networks.

6.2 Higher-order Kuramoto dynamics

The higher-order Kuramoto model [30] describes the synchronization of topological signals defined on simplices of dimension n. For instance, one can consider topological signals defined on the links of a simplicial complex (case $n = 1$) or alternatively one can consider signals defined on the triangles of a simplicial complex (case $n = 2$). The higher-order Kuramoto model is the most natural extension of the Kuramoto model to capture the synchronization of higher-order topological signals.

The standard Kuramoto dynamics describes the dynamics of the phases $\boldsymbol{\theta}$ associated with the nodes of the network. This dynamics, defined by Eq. (25), can be expressed in terms of the incidence matrix $\boldsymbol{B}_{[1]}$ (see Appendix) as

$$\dot{\boldsymbol{\theta}} = \boldsymbol{\omega} - \sigma \boldsymbol{B}_{[1]} \sin \boldsymbol{B}_{[1]}^T \boldsymbol{\theta}. \tag{32}$$

The higher-order Kuramoto dynamics describes instead the dynamics of topological signals $\boldsymbol{\phi}$ with ϕ_α indicating the phase associated with the simplex α of dimension $n > 0$. Therefore, using the insights coming from algebraic topology, the natural definition of the *simple higher-order Kuramoto model* is

$$\dot{\boldsymbol{\phi}} = \hat{\boldsymbol{\omega}} - \sigma \boldsymbol{B}_{[n+1]} \sin \boldsymbol{B}_{[n+1]}^T \boldsymbol{\phi} - \sigma \boldsymbol{B}_{[n]}^T \sin \boldsymbol{B}_{[n]} \boldsymbol{\phi}, \tag{33}$$

where $\hat{\boldsymbol{\omega}}$ is the vector of intrinsic frequencies $\hat{\omega}_\alpha$ associated with each n-dimensional simplex α drawn independently from a normal distribution, i.e., $\hat{\omega}_\alpha \sim \mathcal{N}(\Omega_1, 1/\tau_1)$. As the standard Kuramoto model can be related to the graph Laplacian via linearization (see Eq. (27)), the higher-order Kuramoto model can be related to the higher-order Laplacian upon linearization, leading to

$$\dot{\boldsymbol{\phi}} = \hat{\boldsymbol{\omega}} - \sigma \mathbf{L}_{[n]} \boldsymbol{\phi}. \tag{34}$$

The higher-order Kuramoto dynamics defined on topological signals $\boldsymbol{\phi}$ associated with n dimensional simplices can be projected on $(n + 1)$ and $(n - 1)$ dimensional simplices by applying to the signals the incidence matrices. For instance a dynamics defined on topological signals associated with links can be projected on nodes or on triangles. Specifically, we have that the projected dynamics $\boldsymbol{\phi}^{[-]}$ on $(n - 1)$-dimensional simplices and the projected dynamics $\boldsymbol{\phi}^{[+]}$ on $(n + 1)$-dimensional

simplices is given by

$$\begin{aligned}\boldsymbol{\phi}^{[-]} &= \mathbf{B}_{[n]}\boldsymbol{\phi},\\ \boldsymbol{\phi}^{[+]} &= \mathbf{B}^{\top}_{[n+1]}\boldsymbol{\phi},\end{aligned} \tag{35}$$

where, for $n = 1$, $\mathbf{B}_{[n]}$ indicates the discrete divergence and $\mathbf{B}^{\top}_{[n+1]}$ indicates the discrete curl. Therefore $\boldsymbol{\phi}^{[-]}$ indicates the irrotational component of $\boldsymbol{\phi}$ while $\boldsymbol{\phi}^{[+]}$ indicates the solenoidal component of $\boldsymbol{\phi}$. For the simple higher-order Kuramoto model defined in Eq. (33), by recalling that $\mathbf{B}^{\top}_{[n+1]}\mathbf{B}^{\top}_{[n]} = \mathbf{0}$ and that $\mathbf{B}_{[n]}\mathbf{B}_{[n+1]} = \mathbf{0}$, it follows that the projected topological signals $\boldsymbol{\phi}^{[-]}$ and $\boldsymbol{\phi}^{[+]}$ obey the uncoupled system of equations

$$\begin{aligned}\dot{\boldsymbol{\phi}}^{[-]} &= \boldsymbol{B}_{[n]}\hat{\boldsymbol{\omega}} - \sigma \boldsymbol{L}^{[\mathrm{up}]}_{[n-1]} \sin\left(\boldsymbol{\phi}^{[-]}\right),\\ \dot{\boldsymbol{\phi}}^{[+]} &= \boldsymbol{B}^{T}_{[n+1]}\hat{\boldsymbol{\omega}} - \sigma \boldsymbol{L}^{[\mathrm{down}]}_{[n+1]} \sin\left(\boldsymbol{\phi}^{[+]}\right).\end{aligned} \tag{36}$$

Therefore, the solenoidal and the irrotational components of the topological signals are decoupled for the simple higher-order Kuramoto model.

The higher-order Kuramoto dynamics is remarkable from two perspectives:

(1)First of all it uses topology to naturally define the higher-order interactions between the topological signals. Indeed the incidence matrices define higher-order interactions with a clear prescription indicating the coupled variables and the sign of their interactions. For example, the higher-order Kuramoto dynamics for $n = 1$ dimensional simplices of the simplicial complex shown in Figure 4 reads

$$\begin{aligned}\dot{\theta}_{[1,2]} &= \hat{\omega}_{[1,2]} - \sigma \sin(\theta_{[2,3]} - \theta_{[1,3]} + \theta_{[1,2]}) - \sigma\left[\sin(\theta_{[1,2]} - \theta_{[2,3]}) + \sin(\theta_{[1,3]} + \theta_{[1,2]})\right],\\ \dot{\theta}_{[1,3]} &= \hat{\omega}_{[1,3]} + \sigma \sin(\theta_{[2,3]} - \theta_{[1,3]} + \theta_{[1,2]}) - \sigma\left[\sin(\theta_{[1,3]} + \theta_{[1,2]}) + \sin(\hat{\theta}_{[3]})\right],\\ \dot{\theta}_{[2,3]} &= \hat{\omega}_{[2,3]} - \sigma \sin(\theta_{[2,3]} - \theta_{[1,3]} + \theta_{[1,2]}) - \sigma\left[\sin(\theta_{[2,3]} - \theta_{[1,2]}) + \sin(\hat{\theta}_{[3]})\right],\\ \dot{\theta}_{[3,4]} &= \hat{\omega}_{[3,4]} - \sigma\left[\sin(\theta_{[3,4]}) - \sin(\hat{\theta}_{[3]})\right],\end{aligned} \tag{37}$$

with $\hat{\theta}_{[3]}$ indicating the three-body interaction

$$\hat{\theta}_{[3]} = \theta_{[13]} + \theta_{[23]} - \theta_{[34]}. \tag{38}$$

Therefore, the choice of the higher-order interactions in the higher-order Kuramoto model is naturally dictated by topology.

(2)The synchronization of the higher-order Kuramoto model is only detectable if the right topological filtering of the data is performed. Indeed the naïve order parameter

$$R_n = \frac{1}{N_{[n]}}\left|\sum_{\alpha=1}^{N_{[n]}} e^{\mathrm{i}\phi_\alpha}\right| \tag{39}$$

associated with the unfiltered topological signal ϕ does not detect any synchronization transition (see Figure 8). Instead, the order parameter associated with the solenoidal and the irrotational components of the topological signal do detect the synchronization transition of the topological signals (see Figure 8). These order parameters are given by

$$R_n^{[-]} = \frac{1}{N_{[n-1]}} \left| \sum_{\alpha=1}^{N_{[n-1]}} e^{\mathrm{i}\phi_\alpha^{[-]}} \right|, \quad R_n^{[+]} = \frac{1}{N_{[n+1]}} \left| \sum_{\alpha=1}^{N_{[n+1]}} e^{\mathrm{i}\phi_\alpha^{[+]}} \right|, \tag{40}$$

or alternatively by

$$R_n^{\downarrow} = \frac{1}{N_{[n]}} \left| \sum_{\alpha=1}^{N_{[n]}} e^{\mathrm{i}\phi_\alpha^{\downarrow}} \right|, \quad R_n^{\uparrow} = \frac{1}{N_{[n]}} \left| \sum_{\alpha=1}^{N_{[n]}} e^{\mathrm{i}\phi_\alpha^{\uparrow}} \right|, \tag{41}$$

where $\phi^{\downarrow} = \mathbf{L}_{[n]}^{[\mathrm{down}]}\phi$ and $\phi^{\uparrow} = \mathbf{L}_{[n]}^{[\mathrm{up}]}\phi$.

The synchronization transition described by the simple higher-order Kuramoto model leads to a continuous transition occurring at zero coupling, i.e., the synchronization threshold is $\sigma_c = 0$ as long as $n > 0$. However, the higher-order Kuramoto model admits a formulation called *explosive higher order Kuramoto model* that displays instead a discontinuous transition at a non zero coupling $\sigma_c > 0$.

The *explosive higher-order Kuramoto dynamics* [12] implements an adaptive coupling of the projected dynamics of $\phi^{[+]}$ and $\phi^{[-]}$ through their global order parameters. The adopted adaptive coupling is inspired by analogous couplings previously applied to multilayer and simple networks [49]. The explosive higher-order Kuramoto model [12] is defined by the system of equations

$$\dot{\phi} = \hat{\omega} - \sigma R^{[-]} \boldsymbol{B}_{[n+1]} \sin \boldsymbol{B}_{[n+1]}^T \phi - \sigma R^{[+]} \boldsymbol{B}_{[n]}^T \sin \boldsymbol{B}_{[n]} \phi. \tag{42}$$

It follows that the dynamics projected on the $(n+1)$ and $(n-1)$-dimensional simplices now obeys the coupled system of equations

$$\begin{aligned} \dot{\phi}^{[+]} &= \boldsymbol{B}_{[n+1]}^T \hat{\omega} - \sigma R^{[-]} \boldsymbol{L}_{[n+1]}^{[\mathrm{down}]} \sin\left(\phi^{[+]}\right), \\ \dot{\phi}^{[-]} &= \boldsymbol{B}_{[n]} \hat{\omega} - \sigma R^{[+]} \boldsymbol{L}_{[n-1]}^{[\mathrm{up}]} \sin\left(\phi^{[-]}\right). \end{aligned} \tag{43}$$

Numerical simulations on the configuration model of simplicial complexes with power-law distribution of generalized degrees reveal that the explosive higher-order Kuramoto model displays a discontinuous phase transition. The nature of the transition confirms the theoretical expectations obtained with an approximate phenomenological approach. This transition is clearly detected by a discontinuity in $R_n^{[+]}$ and $R_n^{[-]}$ and in $R_n^{\downarrow}$ and $R_n^{\uparrow}$ as well, but is not captured by the naïve order parameter R_n (see Fig. 8).

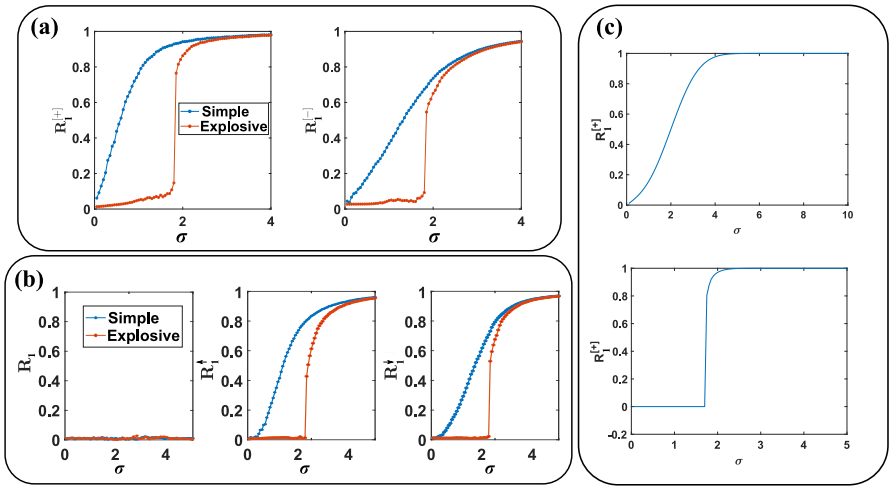


Fig. 8 Higher-order Kuramoto dynamics. The synchronization of higher-order topological signals is captured by the simple and explosive higher-order Kuramoto models. **Panel (a)** The order parameters $R_1^{[+]}$ and $R_1^{[-]}$ reveal the synchronization transition of topological signals defined on links ($n = 1$) of the configuration model of simplicial complexes. **Panel (b)** The naïve order parameter R_1 does not reveal the synchronization transition of topological signals defined on the links of the configuration model of simplicial complex, while the order parameters $R_1^{\uparrow}$ and $R_1^{\downarrow}$, sensible to the irrotational and solenoidal decomposition of the signal, do reveal the transition (as well as $R_1^{[+]}$ and $R_1^{[-]}$ shown in panel (**a**)). The underlying network is the same for both panels and has $N_{[0]} = 1000$ nodes, $N_{[1]} = 5299$ links and $N_{[2]} = 4147$ triangles. The generalized degree of the nodes is power-law distributed with power-law exponent $\gamma = 2.8$. **Panel (c)** shows the theoretical expectations provided by an effective phenomenological model treated in Ref. [12] for the simple (top) and explosive (bottom) higher-order Kuramoto models. Reprinted figure with permission from Ref. [12]. ©Copyright (2020) by the American Physical Society.

In Ref. [12] it has been shown that the nature of the phase transition does not change if the generalized degree distribution is more uniform or if the simplicial complex has a non trivial network geometry. Interestingly, simple and explosive higher-order Kuramoto models can be investigated on simplicial complexes constructed from real connectomes leading to continuous (for the simple higher-order Kuramoto model) and discontinuous (for the explosive higher-order Kuramoto model) synchronization transitions.

6.3 Coupled topological signals

So far we have considered the synchronization of topological signals defined on simplices of dimension $n > 0$. However, topological signals associated with simplices of different dimension can co-exist and co-evolve. For instance, phases associated with the nodes of a simplicial complex can be coupled with phases associated with

its links. In this section we will show how different topological signals, i.e., phases defined on simplicial complexes of different dimensions, can be coupled to each other leading to simultaneous explosive synchronization transitions. For simplicity of presentation we will focus on phases defined on nodes and links, but we emphasize that our formalism allows one to consider the interaction of more general topological signals.

We start by considering Model 1, an explosive higher-order Kuramoto model of coupled signals of nodes and links. This model differs from the explosive higher-order Kuramoto model defined in the previous section as it includes an additional adaptive coupling among the topological signals of nodes and links, and obeys the equations

$$\begin{aligned}\dot{\boldsymbol{\theta}} &= \boldsymbol{\omega} - \sigma R_1^{[-]} \mathbf{B}_{[1]} \sin(\mathbf{B}_{[1]}^{\top}\boldsymbol{\theta}),\\ \dot{\boldsymbol{\phi}} &= \hat{\boldsymbol{\omega}} - \sigma R_0 R_1^{[+]} \mathbf{B}_{[1]}^{\top} \sin(\mathbf{B}_{[1]}\boldsymbol{\phi}) - R_1^{[-]} \sigma \mathbf{B}_{[2]} \sin(\mathbf{B}_{[2]}^{\top}\boldsymbol{\phi}).\end{aligned} \tag{44}$$

This model simulated in a wide variety of simplicial complexes including the NGF, the configuration model of simplicial complexes, and the clique complex of real connectomes displays a simultaneous explosive (i.e., discontinuous) synchronization of the topological signals defined on nodes and of the soleinodal and irrotational component of the topological signals defined on links [47]. Indeed, at a critical threshold $\sigma = \sigma_c$ we observe a discontinuity in the three order parameters R_0, $R_1^{[-]}$ and $R_1^{[+]}$. In Figure 9 we present numerical evidence of this discontinuous transition by displaying the corresponding hysteresis loop in the order parameters. In particular, instead of plotting the order parameters obtained at each value of σ starting from random initial conditions as in Figure 8 here we display the order parameters along the forward and backward synchronization transitions obtained by first adiabatically increasing and then decreasing the coupling constant σ.

Interestingly, this model (Model 1) admits a variation (Model 2) that describes the simultaneous synchronization of the topological signals associated with the nodes and the irrotational component of the topological signal associated with the links. This simpler version of the explosive higher-order Kuramoto model of coupled topological signals can be also defined on pairwise networks and is amenable to an exact analytical treatment on fully connected networks and to an accurate annealed approximation solution on random networks with a given degree distribution. More specifically, Model 2 only couples the signal of the nodes with the signal of the links projected to the nodes, as described by the differential equations

$$\dot{\boldsymbol{\theta}} = \boldsymbol{\omega} - \sigma R_1^{[-]} \mathbf{B}_{[1]} \sin(\mathbf{B}_{[1]}^{\top}\boldsymbol{\theta}), \tag{45}$$

$$\dot{\boldsymbol{\phi}} = \hat{\boldsymbol{\omega}} - \sigma R_0 \mathbf{B}_{[1]}^{\top} \sin(\mathbf{B}_{[1]}\boldsymbol{\phi}) - \sigma \mathbf{B}_{[2]} \sin(\mathbf{B}_{[2]}^{\top}\boldsymbol{\phi}). \tag{46}$$

Projecting the dynamics of the link phases down to 0-simplices as in the previous section, we introduce $\boldsymbol{\psi}$ for simplicity of notation with

$$\boldsymbol{\psi} \equiv \boldsymbol{\phi}^{[-]} = \mathbf{B}_{[1]}\boldsymbol{\phi}. \tag{47}$$

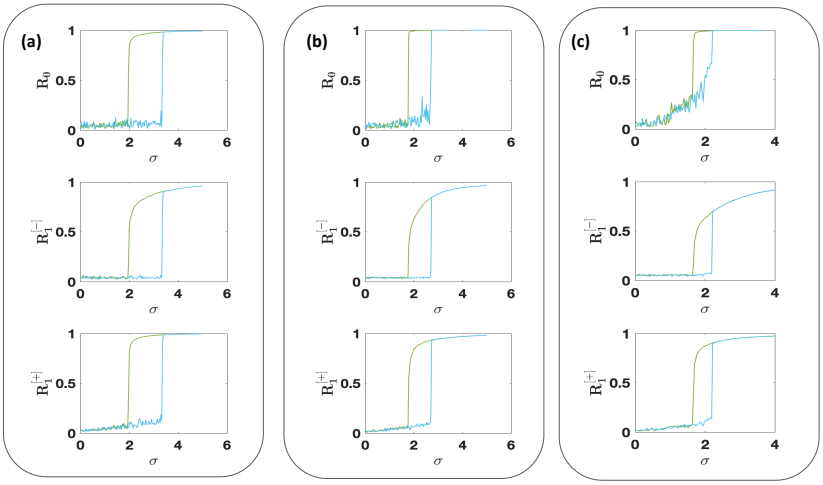


Fig. 9 Simultaneous explosive synchronization of coupled topological signals. Model 1 displays the simultaneous explosive (discontinuous) transition captured by the order parameters R_0, $R_1^{[-]}$ and $R_1^{[+]}$. **Panels (a), (b), and (c)** provide numerical evidence of this discontinuous transition on different simplicial network topologies: the NGF with flavor $s = -1$ and dimension d (panel (**a**)), the configuration model of pure $d = 3$ simplicial complex with power-law generalized degree distribution with power-law exponent $\gamma = 2.8$ (panel (**b**)) and the clique complex of the Caenorhabditis elegans (C.elegans) connectome coming from Ref. [50] (panel (**c**)). Figure adapted from [47].

By left multiplying Eq. (46) by $\mathbf{B}_{[1]}$, we obtain the closed system of equations for $\boldsymbol{\theta}$ and $\boldsymbol{\psi}$

$$\begin{aligned}\dot{\boldsymbol{\theta}} &= \boldsymbol{\omega} - \sigma R_1^{[-]} \mathbf{B}_{[1]} \sin(\mathbf{B}_{[1]}^{\top} \boldsymbol{\theta}),\\ \dot{\boldsymbol{\psi}} &= \tilde{\boldsymbol{\omega}} - \sigma R_0 \mathbf{L}_{[0]} \sin(\boldsymbol{\psi}),\end{aligned} \tag{48}$$

where $\tilde{\boldsymbol{\omega}} = \mathbf{B}_{[1]} \hat{\boldsymbol{\omega}}$. Here we assume $\omega \sim \mathcal{N}(0,1)$ and $\hat{\omega}_\alpha \sim \mathcal{N}(\Omega_1, 1/\tau_1)$. With these hypotheses the internal frequencies of the links projected on the nodes $\{\tilde{\omega}_i\}_{i=1,2,\ldots,N_{[0]}}$ are Gaussian correlated variables with average

$$\langle \tilde{\omega}_i \rangle = \left[\sum_{j<i} a_{ij} - \sum_{j>i} a_{ij} \right] \Omega_1 \tag{49}$$

and with correlation matrix $\mathbf{C}$ of elements $C_{ij} = \left\langle \tilde{\omega}_i \tilde{\omega}_j \right\rangle - \langle \tilde{\omega}_i \rangle \left\langle \tilde{\omega}_j \right\rangle$ given by

$$\mathbf{C} = \mathbf{L}_{[0]} \frac{1}{\tau_1^2}. \tag{50}$$

To understand the nature of the synchronization transition analytically when Model 2 is defined on an uncorrelated random graph, in the following we discuss the solution

of the model in the *annealed approximation*. The annealed approximation is a widely used approximation to study dynamical processes on random uncorrelated networks which consists in substituting the adjacency matrix entries of the network a_{ij} by their average values in an uncorrelated random network with given degree sequence, i.e.,

$$a_{ij} \to \frac{k_i k_j}{\langle k \rangle N}. \tag{51}$$

Using this approximation, Eqs. (48) can be recast into the differential equations

$$\begin{aligned} \dot{\boldsymbol{\theta}} &= \boldsymbol{\omega} - \sigma R_1^{[-]} \hat{R}_0 \mathbf{k} \cdot \sin(\boldsymbol{\theta} - \hat{\Theta}), \\ \dot{\boldsymbol{\psi}} &= \tilde{\boldsymbol{\omega}} + \sigma R_0 \hat{R}_1^{[-]} \mathbf{k} \sin \hat{\Psi} - \sigma R_0 \mathbf{k} \odot \sin \boldsymbol{\psi}, \end{aligned} \tag{52}$$

where $\odot$ indicates the Hadamard product (element by element multiplication) and where two auxiliary complex order parameters are defined as

$$\hat{R}_0 e^{\mathrm{i}\hat{\Theta}} = \sum_{i=1}^{N_{[0]}} \frac{k_i}{\langle k \rangle N_{[0]}} e^{\mathrm{i}\theta_i}, \quad \hat{R}_1^{[-]} e^{\mathrm{i}\hat{\Psi}} = \sum_{i=1}^{N_{[0]}} \frac{k_i}{\langle k \rangle N_{[0]}} e^{\mathrm{i}\psi_i}, \tag{53}$$

with $\hat{R}_0, \hat{\Theta}, \hat{R}_1^{[-]}$ and $\hat{\Psi}$ being real. Let us indicate with $g(\omega)$ the probability distribution of the internal frequencies of the nodes and with $G_i(\tilde{\omega})$ the marginal probability distribution of the internal frequencies of the links projected on node i, i.e., the marginal probability that $\tilde{\omega}_i = \tilde{\omega}$. With this notation it is possible to derive the analytic solution of Eqs. (52) which gives the following expression for the order parameters

$$\begin{aligned} R_0 &= \frac{1}{N_{[0]}} \sum_{i=1}^{N_{[0]}} r_0(i), \qquad \hat{R}_n = \sum_{i=1}^{N_{[0]}} \frac{k_i}{\langle k \rangle N_{[0]}} r_0(i), \\ R_1^{[-]} &= \frac{1}{N_{[0]}} \sum_{i=1}^{N_{[0]}} r_1^{[-]}(i), \qquad \hat{R}_1^{[-]} = \sum_{i=1}^{N_{[0]}} \frac{k_i}{\langle k \rangle N_{[0]}} r_1^{[-]}(i), \end{aligned} \tag{54}$$

with $r_0(i)$ and $r_1^{[-]}(i)$ given by

$$\begin{aligned} r_0(i) &= \int_{|\hat{c}_i|<1} d\omega g(\omega) \sqrt{1 - \left(\frac{\omega - \Omega_0}{\sigma k_i \hat{R}_0 R_1^{[-]}} \right)^2}, \\ r_1^{[-]}(i) &= \int_{|\hat{d}_i|<1} d\tilde{\omega} G_i(\tilde{\omega}) \sqrt{1 - \left(\frac{\tilde{\omega}}{\sigma k_i \hat{R}_0} \right)^2}, \end{aligned} \tag{55}$$

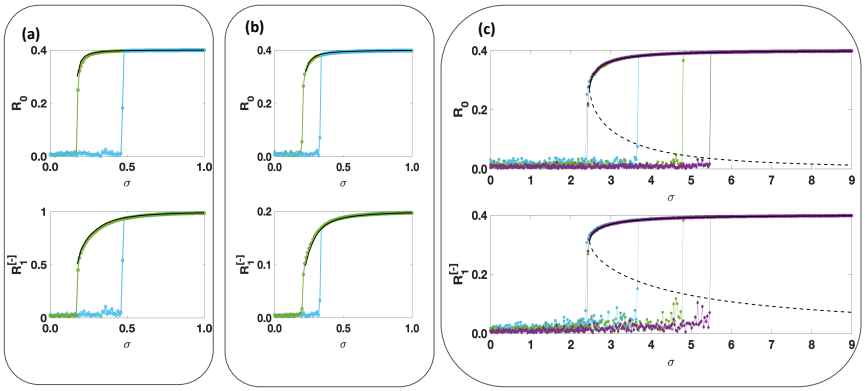


Fig. 10 Theoretical prediction for Model 2 of explosive higher-order Kuramoto model of coupled dynamical signals applied to random and fully connected networks. The hysteresis loop for Model 2 is shown for different types of networks. The backward transition is fully captured by the theoretical expectations (solid black lines). **Panels (a), (b)** and **(c)** show the order parameters R_1 and $R_1^{[-]}$ versus the coupling constant σ for: A Poisson network with average degree $c = 12$ and $N_{[0]} = 1600$ nodes (panel (**a**)), a scale-free network with minimum degree $m = 6$, power-law exponent $\gamma = 2.5$ and $N_{[0]} = 1600$ nodes (panel (**b**)) and a fully connected network of different network sizes $N_{[0]} = 500$ (cyan symbols), $N_{[0]} = 1000$ (green symbols)and $N_{[0]} = 2000$ (purple symbols) (panel (**c**)). From panel (**c**) it is evident that the forward transition occurs at higher values of σ for larger network size, confirming the theoretical prediction indicating that the transition is driven by finite size effects and it is absent in the infinite network limit. Figures adapted from [47].

and $\hat{c}_i$ and $\hat{d}_i$ indicating

$$\hat{c}_i = \frac{\omega - \Omega_0}{\sigma k_i \hat{R}_0 R_1^{[-]}}, \quad \hat{d}_i = \frac{\tilde{\omega}}{\sigma k_i \hat{R}_0}. \tag{56}$$

Figure 10 shows excellent agreement between the simulation results of Model 2 and the analytical prediction obtained in the annealed approximation for a Poisson network with average degree $c = 12$ (panel (**a**)) and for an uncorrelated scale-free network with minimum degree $m = 6$ and power-law exponent $\gamma = 2.5$ (panel (**b**)).

Model 2 of explosive higher-order synchronization of coupled topological signals of nodes and links can be also solved exactly on a fully connected network. Before discussing these theoretical results let us highlight that when treating Model 2 on a fully connected network the model parameters need to be rescaled appropriately to give a well defined transition in the large network limit. In particular the coupling constant σ and τ_1 are rescaled to

$$\sigma \to \frac{\sigma}{N},$$
$$\tau_1 \to \tau_1 \sqrt{N}. \tag{57}$$

Moreover, for simplicity we set $\Omega_1 = 0$. With these hypotheses the marginal distribution $G_i(\tilde{\omega}) = G(\tilde{\omega})$ for every node i of the network can be derived to be equal to

$$G(\tilde{\omega}) = \frac{\tau_1}{\sqrt{2\pi/\bar{c}}} \exp\left[-\tau_1^2 \bar{c} \frac{\tilde{\omega}^2}{2}\right], \tag{58}$$

with $\bar{c} = N/(N-1)$. The self-consistent equations for the order parameters $R_0 = \hat{R}_0$ and $R_1^{[-]} = \hat{R}_1^{[-]}$ are given by

$$1 = \sigma R_1^{[-]} h\left(\sigma^2 R_0^2 (R_1^{[-]})^2\right),$$
$$R_1^{[-]} = \sigma R_0 \tau_1 \sqrt{\bar{c}} h\left(\sigma^2 \tau_1^2 R_0^2\right), \tag{59}$$

where the scaling function $h(x)$ is given by

$$h(x) = \sqrt{\frac{\pi}{2}} e^{-x/4} \left[I_0\left(\frac{x}{4}\right) + I_1\left(\frac{x}{4}\right)\right], \tag{60}$$

with I_0 and I_1 indicating the modified Bessel functions.

These equations agree perfectly well with direct simulation of Model 2 dynamical Eqs. (46) on a fully connected network as it can be appreciated from Figure 10(c). Moreover a closer look to these equations reveals an important aspect of these transitions. While the backward transition has a well defined limit as $N \to \infty$, the forward transition occurs at larger value of the coupling constant for large network size N, and is only determined by finite size fluctuations, therefore the transition disappears in the limit $N \to \infty$. Interestingly, this lack of a proper hysteresis loop can be also predicted for Model 2 defined on uncorrelated random graphs with finite second moment of the degree distribution, starting from their annealed approximation solution.

7 Conclusions

In this chapter our goal has been to provide evidence that the interplay between simplicial complex structure and dynamics is mediated by simplicial geometry and topology. The spectral properties of the graph Laplacian and the higher-order Laplacian have been used here to reveal how simplicial synchronization is shaped by topological and geometry of the simplicial complex. In particular, we investigated how simplicial network geometry changes the phase diagram of the Kuramoto model defined on the network skeleton of simplicial complexes with notable geometrical

properties and characterized by a finite spectral dimension. We have shown that a spectral dimension smaller or equal than four but larger than two can lead to a regime of frustrated synchronization characterized by large spatio-temporal fluctuations of the order parameter, while a spectral dimension smaller or equal than two leads to a Kuramoto model in the incoherent state for every finite value of the coupling constant. These theoretical results have been shown to apply to the simplicial complexes generated by the modelling framework called Network Geometry with Flavor (NGF) that is able to generate simplicial complexes with tunable spectral dimension of the graph Laplacian. Interestingly, the NGF are characterized also by displaying higher-order spectral dimension of the higher-order up Laplacian that describe higher-order diffusion processes.

This chapter introduces also a set of models for capturing synchronization of topological signals, i.e., phases not only associated with the nodes of a simplicial complex but also to the higher-order simplices such as links, triangles, and so on. This higher-order synchronization reveals itself in the order parameter of the irrotational and solenoidal projection of the topological signals. In the simple higher-order Kuramoto model the irrotational and solenoidal projection of the topological signal are uncoupled and undergo a sychronization transition at $\sigma_c = 0$. However, when these two projections are coupled to each other by an adaptive global coupling the synchronization becomes explosive, i.e., discontinuous, and occurs at a non-zero value of coupling constant.

The higher-order Kuramoto model can be further extended to capture coupled topological signals of different dimension, for instance coupling phases associated with nodes and to links of a network or of a simplicial complex. This generalized higher-order Kuramoto model can lead to an explosive phase transition affecting simultaneously the phases associated with the nodes and the irrotational and solenoidal projection of the phases associated with the links. Interestingly, the higher-order Kuramoto model of coupled topological signals defined on nodes and links can be treated analytically using the annealed approximation when it is defined on a random uncorrelated network and can be solved exactly on a fully connected network. This solution confirms the discontinuous nature of the transition of the explosive higher-order Kuramoto model and sheds light on the stability of the hysteresis loop associated with the transition on finite networks. The mathematical framework that we have proposed here can be explored and modified in different directions and we believe that an in-depth analysis of the model and its variations will provide important insights on the interplay between topology and dynamics. For instance, we note that the higher-order Kuramoto model has been recently modified [51] to investigate also the properties of a consensus model finding interesting results.

In conclusion, this chapter aims to provide an overview of the relation between network geometry topology and dynamics. We believe this topic will flourish in the incoming years and will transform our understanding of the relation between structure and dynamics of higher-order networks. Therefore our expectation is that this research line will play a relevant role for providing new insights in a variety of applications including brain dynamics and biological transportation networks.

References

1. Albert László Barabási. *Network Science*. Cambridge University press, 2016.
2. Sergey N Dorogovtsev, Alexander V Goltsev, and José FF Mendes. Critical phenomena in complex networks. *Reviews of Modern Physics*, 80(4):1275, 2008.
3. Alain Barrat, Marc Barthelemy, and Alessandro Vespignani. *Dynamical processes on complex networks*. Cambridge University Press, 2008.
4. Federico Battiston, Giulia Cencetti, Iacopo Iacopini, Vito Latora, Maxime Lucas, Alice Patania, Jean-Gabriel Young, and Giovanni Petri. Networks beyond pairwise interactions: structure and dynamics. *Physics Reports*, 2020.
5. Ginestra Bianconi. *Higher-order networks: An introduction to simplicial complexes*. Cambridge University Press, 2021.
6. Ginestra Bianconi. Interdisciplinary and physics challenges of network theory. *EPL (Europhysics Letters)*, 111(5):56001, 2015.
7. Leo Torres, Ann S Blevins, Danielle S Bassett, and Tina Eliassi-Rad. The why, how, and when of representations for complex systems. *arXiv preprint arXiv:2006.02870*, 2020.
8. Steven H Strogatz. From kuramoto to crawford: exploring the onset of synchronization in populations of coupled oscillators. *Physica D: Nonlinear Phenomena*, 143(1-4):1–20, 2000.
9. Alex Arenas, Albert Díaz-Guilera, Jurgen Kurths, Yamir Moreno, and Changsong Zhou. Synchronization in complex networks. *Physics Reports*, 469(3):93–153, 2008.
10. Stefano Boccaletti, Alexander N Pisarchik, Charo I Del Genio, and Andreas Amann. *Synchronization: from coupled systems to complex networks*. Cambridge University Press, 2018.
11. Yoshiki Kuramoto. Self-entrainment of a population of coupled non-linear oscillators. In Huzihiro Araki, editor, *International Symposium on Mathematical Problems in Theoretical Physics*, pages 420–422, Berlin, Heidelberg, 1975. Springer Berlin Heidelberg.
12. Ana P Millán, Joaquín J Torres, and Ginestra Bianconi. Explosive higher-order kuramoto dynamics on simplicial complexes. *Physical Review Letters*, 124(21):218301, 2020.
13. Joaquín J Torres and Ginestra Bianconi. Simplicial complexes: higher-order spectral dimension and dynamics. *Journal of Physics: Complexity*, 1(1):015002, 2020.
14. Sergio Barbarossa and Stefania Sardellitti. Topological signal processing over simplicial complexes. *IEEE Transactions on Signal Processing*, 68:2992–3007, 2020.
15. Owen T Courtney and Ginestra Bianconi. Generalized network structures: the configuration model and the canonical ensemble of simplicial complexes. *Physical Review E*, 93(6):062311, 2016.
16. Ginestra Bianconi and Christoph Rahmede. Network geometry with flavor: from complexity to quantum geometry. *Physical Review E*, 93(3):032315, 2016.
17. Ginestra Bianconi and Christoph Rahmede. Emergent hyperbolic network geometry. *Scientific Reports*, 7:41974, 2017.
18. Daan Mulder and Ginestra Bianconi. Network geometry and complexity. *Journal of Statistical Physics*, 173(3-4):783–805, 2018.
19. Owen T. Courtney and Ginestra Bianconi. Weighted growing simplicial complexes. *Physical Review E*, 95(6):062301, 2017.
20. Per Sebastian Skardal and Alex Arenas. Abrupt desynchronization and extensive multistability in globally coupled oscillator simplexes. *Physical review letters*, 122(24):248301, 2019.
21. Per Sebastian Skardal and Alex Arenas. Higher-order interactions in complex networks of phase oscillators promote abrupt synchronization switching. *arXiv preprint arXiv:1909.08057*, 2019.
22. Per Sebastian Skardal and Alex Arenas. Memory selection and information switching in oscillator networks with higher-order interactions. *Journal of Physics: Complexity*, 2020.
23. Repository for higher-order network codes.
24. Mikhael Gromov. Hyperbolic groups. In *Essays in group theory*, pages 75–263. Springer, 1987.
25. Ana P Millán, Reza Ghorbanchian, Nicolò Defenu, Federico Battiston, and Ginestra Bianconi. Local topological moves determine global diffusion properties of hyperbolic higher-order networks. *arXiv preprint arXiv:2102.12885*, 2021.

26. Raffaella Burioni and Davide Cassi. Random walks on graphs: ideas, techniques and results. *Journal of Physics A: Mathematical and General*, 38(8):R45, 2005.
27. Rammal Rammal and Gérard Toulouse. Random walks on fractal structures and percolation clusters. *Journal de Physique Lettres*, 44(1):13–22, 1983.
28. Raffaella Burioni and Davide Cassi. Universal properties of spectral dimension. *Physical Review Letters*, 76(7):1091, 1996.
29. Zhihao Wu, Giulia Menichetti, Christoph Rahmede, and Ginestra Bianconi. Emergent complex network geometry. *Scientific Reports*, 5:10073, 2015.
30. Ana P Millán, Giacomo Gori, Federico Battiston, Tilman Enss, and Nicolò Defenu. Complex networks with tuneable dimensions as a universality playground. *arXiv preprint arXiv:2006.10421*, 2020.
31. Marija Mitrović Dankulov, Bosiljka Tadić, and Roderick Melnik. Spectral properties of hyperbolic nanonetworks with tunable aggregation of simplexes. *Physical Review E*, 100(1):012309, 2019.
32. Ana P Millán, Joaquín J Torres, and Ginestra Bianconi. Synchronization in network geometries with finite spectral dimension. *Phys. Rev. E*, 99(2):022307, 2019.
33. A P Millán, J J Torres, and G Bianconi. Complex network geometry and frustrated synchronization. *Scientific Reports*, 8(9910), 2018.
34. Abubakr Muhammad and Magnus Egerstedt. Control using higher order laplacians in network topologies. In *Proc. of 17th International Symposium on Mathematical Theory of Networks and Systems*, pages 1024–1038. Citeseer, 2006.
35. Timothy E Goldberg. Combinatorial laplacians of simplicial complexes. *Senior Thesis, Bard College*, 2002.
36. Joaquín J Torres and J Marro. Brain performance versus phase transitions. *Scientific Reports*, 5:12216, 2015.
37. Marcus Reitz and Ginestra Bianconi. The higher-order spectrum of simplicial complexes: a renormalization group approach. *Journal of Physics A: Mathematical and Theoretical*, 2020.
38. Juan A Acebrón, Luis L Bonilla, Conrad J Pérez Vicente, Félix Ritort, and Renato Spigler. The kuramoto model: a simple paradigm for synchronization phenomena. *Reviews of Modern Physics*, 77(1):137, 2005.
39. Juan G Restrepo, Edward Ott, and Brian R Hunt. Onset of synchronization in large networks of coupled oscillators. *Physical Review E*, 71(3):036151, 2005.
40. M Chavez, D-U Hwang, A Amann, HGE Hentschel, and S Boccaletti. Synchronization is enhanced in weighted complex networks. *Physical Review Letters*, 94(21):218701, 2005.
41. Weiyu Huang, Thomas AW Bolton, John D Medaglia, Danielle S Bassett, Alejandro Ribeiro, and Dimitri Van De Ville. A graph signal processing perspective on functional brain imaging. *Proceedings of the IEEE*, 106(5):868–885, 2018.
42. Miguel Ruiz-Garcia and Eleni Katifori. Topologically controlled emergent dynamics in flow networks. *arXiv preprint arXiv:2001.01811*, 2020.
43. H Hong, Hyunggyu Park, and M Y Choi. Collective synchronization in spatially extended systems of coupled oscillators with random frequencies. *Physical Review E*, 72(3):036217, 2005.
44. Hyunsuk Hong, Hugues Chaté, Hyunggyu Park, and Lei Han Tang. Entrainment transition in populations of random frequency oscillators. *Physical Review Letters*, 99(18):184101, 2007.
45. Paolo Moretti and Miguel A Muñoz. Griffiths phases and the stretching of criticality in brain networks. *Nature Communications*, 4:2521, 2013.
46. Pablo Villegas, Paolo Moretti, and Miguel A Muñoz. Frustrated hierarchical synchronization and emergent complexity in the human connectome network. *Scientific Reports*, 4:5990, 2014.
47. Reza Ghorbanchian, Juan G Restrepo, Joaquín J Torres, and Ginestra Bianconi. Higher-order simplicial synchronization of coupled topological signals. *arXiv preprint arXiv:2011.00897*, 2020.
48. Jason W Rocks, Andrea J Liu, and Eleni Katifori. Revealing structure-function relationships in functional flow networks via persistent homology. *Physical Review Research*, 2(3):033234, 2020.

49. Xiyun Zhang, Stefano Boccaletti, Shuguang Guan, and Zonghua Liu. Explosive synchronization in adaptive and multilayer networks. *Physical review letters*, 114(3):038701, 2015.
50. Lav R Varshney, Beth L Chen, Eric Paniagua, David H Hall, and Dmitri B Chklovskii. Structural properties of the caenorhabditis elegans neuronal network. *PLoS Comput Biol*, 7(2):e1001066, 2011.
51. Lee DeVille. Consensus on simplicial complexes, or: The nonlinear simplicial laplacian. *arXiv preprint arXiv:2010.07421*, 2020.

Appendix: Kuramoto dynamics expressed in terms of the incidence matrix

In this Appendix our aim is to show that Eq. (25) that we rewrite here for convenience,

$$\dot{\theta}_i = \omega_i + \sigma \sum_{j=1}^{N_{[0]}} a_{ij} \sin\left(\theta_j - \theta_i\right), \tag{61}$$

is equivalent to Eq. (32) given by

$$\dot{\boldsymbol{\theta}} = \boldsymbol{\omega} - \sigma \boldsymbol{B}_{[1]} \sin \boldsymbol{B}_{[1]}^T \boldsymbol{\theta}. \tag{62}$$

In order to show this let us observe that the incidence matrix $\mathbf{B}_{[1]}$ has elements given by

$$[B_{[1]}]_{i\ell} = \begin{cases} -1 \text{ if } \ell = [i,j], \\ 1 \text{ if } \ell = [j,i], \\ 0 \text{ otherwise.} \end{cases} \tag{63}$$

To show the equivalence between Eq. (61) and Eq. (62) let us start by rewriting Eq. (62) element by element, getting

$$\dot{\theta}_i = \omega_i - \sigma \sum_{\ell \in S_1} [B_{[1]}]_{i\ell} \sin\left(\sum_{j \in S_0} [B_{[1]}^\top]_{\ell j} \theta_j\right), \tag{64}$$

where we indicate with S_1 the set of all links present in the simplicial complex or network under consideration.

Let us consider the particular link $\ell = [i,j]$ in this case we have

$$[B_{[1]}]_{i\ell} \sin\left(\sum_{j \in S_0} [B_{[1]}^\top]_{\ell j} \theta_j\right) = -a_{ij} \sin(\theta_j - \theta_i). \tag{65}$$

Equivalently, if we consider the same link with opposite orientation $\ell = [j,i]$ we get

$$[B_{[1]}]_{i\ell} \sin\left(\sum_{j\in S_0} [B^{\top}_{[1]}]_{\ell j}\theta_j\right) = a_{ij}\sin(\theta_i-\theta_j) = -a_{ij}\sin(\theta_j-\theta_i). \quad (66)$$

Since the incidence matrix $\mathbf{B}_{[1]}$ has non-zero elements only among nodes and links incident to each other, it follows that Eq. (61) is equivalent to Eq. (62).